Celestially determined annual seasonality of equatorial tropical rain forests

Kanehiro Kitayama[*]*, Masayuki Ushio*[†,‡,§]*, Shin-ichiro Aiba*[¶]

Abstract

Annual vegetative periodicity is not well known in equatorial tropical rain forests except for photoperiodically induced or El-Niño-drought induced synchronous flowering/fruiting. The lack of vegetative periodicity such as leaf flush and fall in these forests has been believed to reflect an "aseasonal" climate. In the present study, we show a distinct annual seasonality in canopy dynamics using a Fourier analysis with a statistical significance test on the long-term, fortnightly monitored dataset of leaf litterfall in nine Bornean evergreen tropical rain forests on Mount Kinabalu. Such periodicity occurs across altitudes and soil types in all years irrespective of the year-to-year climatic variability, suggesting that regional climatic factors rather than local edaphic and/or biotic conditions cause the precise 1-year periodicity. We examine climatic factors that have causative effects on the distinct 1-year periodicity using a newly developed spectrum convergent cross mapping analysis that can distinguish causal relationships from seasonality-driven synchronization. We find that mean daily air temperature is most strongly, causatively related to the 1-year periodicity of leaf litterfall. We suggest that annual temperature changes in association with the movement of the intertropical convergence zone cause the distinct annual vegetative periodicity. Because vegetative periodicity can be transmitted to the dynamics of higher trophic levels through a trophic cascade, interactions between vegetative periodicity and daily air temperature, not rainfall, would more strongly cause changes in the dynamics of forest ecosystems. Our results show that we need to redefine our concept of equatorial "aseasonal" tropical rain forests, and that air temperature is a more important factor than other climate variables in the climate-forest ecosystem interaction.

Keywords: *equatorial tropical forests; convergent cross mapping; Fourier analysis; Mount Kinabalu; seasonality; time series analysis*

K.K. and M.U. contributed equally to this work. Correspondence and requests for materials should be addressed to K.K. (kanehiro@kais.kyoto-u.ac.jp) and M.U. (ong8181@gmail.com).

Introduction

One of the most well-defined characteristics of the equatorial tropical rain-forest climate is the lack of clear annual changes in mean monthly temperature, while monthly rainfall always exceeds monthly potential evapotranspiration (Whitmore 1975). This hot and humid climate throughout the year without marked seasonality supports vegetative growth year round in tropical rain forests, leading to high primary productivity (Whitmore 1975). In spite of the year-round constant climate,

[*]Graduate School of Agriculture, Kyoto University, Kyoto 606-8502, Japan
[†]Hakubi Center, Kyoto University, Kyoto 606-8501, Japan
[‡]Center for Ecological Research, Kyoto University, Otsu 520-2113, Japan
[§]PRESTO, Japan Science and Technology Agency, Kawaguchi 332-0012, Japan
[¶]Graduate School of Science and Engineering, Kagoshima University, Kagoshima 890-0065, Japan

tropical trees are known to show synchronous flowering and fruiting in the Neotropics (Borchert et al. 2005), Southeast Asia (Sakai 2002, Sakai et al. 2006) and Africa (Adamescu et al. 2018). Annual photoperiodicity (Borchert et al. 2005) or seasonal radiation change (Wright and Calderón 2018) has been suggested to trigger reproductive synchrony as an annual event in the Amazon and elsewhere. On the other hand, irregular El Niño droughts are suggested to trigger supra-annual flowering and fruiting in Southeast Asian tropical rain forests, the phenomenon known as masting or general flowering (Sakai 2002, Sakai et al. 2006). Synchronous reproduction is believed to be evolutionarily favourable for promoting outcrossing among sparsely distributed trees within a species in tropical rain forests, because the density of conspecific trees is extremely low there, reflecting the high tree-species diversity (Sakai et al. 1999). Thus, phenological changes in reproduction in such "aseasonal" rain forests have evolutional significance through enhancing genetic exchanges. Phenological changes in vegetative activities such as leaf flush and fall must also have significant consequences in tropical ecosystems, because synchronous leaf flush and fall influence biological interactions in grazing food-chains and detritus food-chains, respectively (Lodge et al. 1994). However, phenological periodicity in the leaf dynamics has not been extensively described in equatorial tropical rain forests (Reich et al. 2004), except in semideciduous tropical forests with a dry season (Rivera et al. 2002).

Results and Discussion

In the present study, we apply a Fourier analysis with a significance test (Bush et al. 2017) to the long-term litterfall and meteorological monitoring data in Bornean tropical rain forests that lack a dry season to examine vegetative and meteorological periodicity. Falling litter in nine forests that differ in altitude (700, 1700, 2700 and 3100 m) and soil types (soils derived from either sedimentary, granitic or ultrabasic rocks) was collected fortnightly between 1996 and 2006 or longer on Mount Kinabalu, Malaysian Borneo (summit height 4095 m; 6° 5′ N, 116 33′ E) (sedimentary/granite site is hereafter referred to as "sedimentary site") (Fig. 1, Table S1). Collected litter was sorted into leaf, reproductive (flowers and fruits combined) and other fractions. Meteorological monitoring was conducted at altitudes similar to those of the forest plots. Nitrogen and phosphorus availability is known to be greater in soils derived from sedimentary rocks than from ultrabasic rocks at the same altitude (Kitayama and Aiba 2002). The annual amount of leaf litterfall varies greatly among the nine forests, reflecting the differences in altitude and soil nutrient availability (Kitayama and Aiba 2002). Forest on sedimentary soils at 700 m has six-fold greater annual leaf litterfall than that on ultrabasic soils at 3100 m (Kitayama and Aiba 2002). Regardless of the variations in altitude, soil type and productivity, all forests show annual sinusoidal patterns of leaf litterfall, although peak values change from year to year within and among forests (Figs. 1, S1). Annual sinusoidal patterns are not evident in the reproductive-litter dynamics (Fig. S2).

Fourier analysis detected the presence of significant 12 mo (or 11.8 mo) length of periodicity in leaf litterfall in all forests except for the 2700-m sedimentary and the 3100-m sedimentary sites, where the dominant cycle was 6.3 and 24 mo, respectively (Figs. 2a–d and S1–S4, Table S2). For the 700-m ultrabasic site, the dominant periodicity was 1 year, but it was not significant due to insufficient length of the time series, and thus we omitted the 700-m ultrabasic site from the subsequent analyses. Exact (or nearly exact) and significant 1-year periodicity occurred irrespective of altitude and soil type in six out of the eight forests, indicating that the periodicity is not influenced by local environmental, biotic conditions, and/or their interactions. By contrast, significant dominant cycles of reproductive-organ litter (flowers and fruits combined) range from 15 mo to more than 48 mo, and periodicity was not consistent across altitudes and soil types (Fig. 2a–d). As for the meteorological

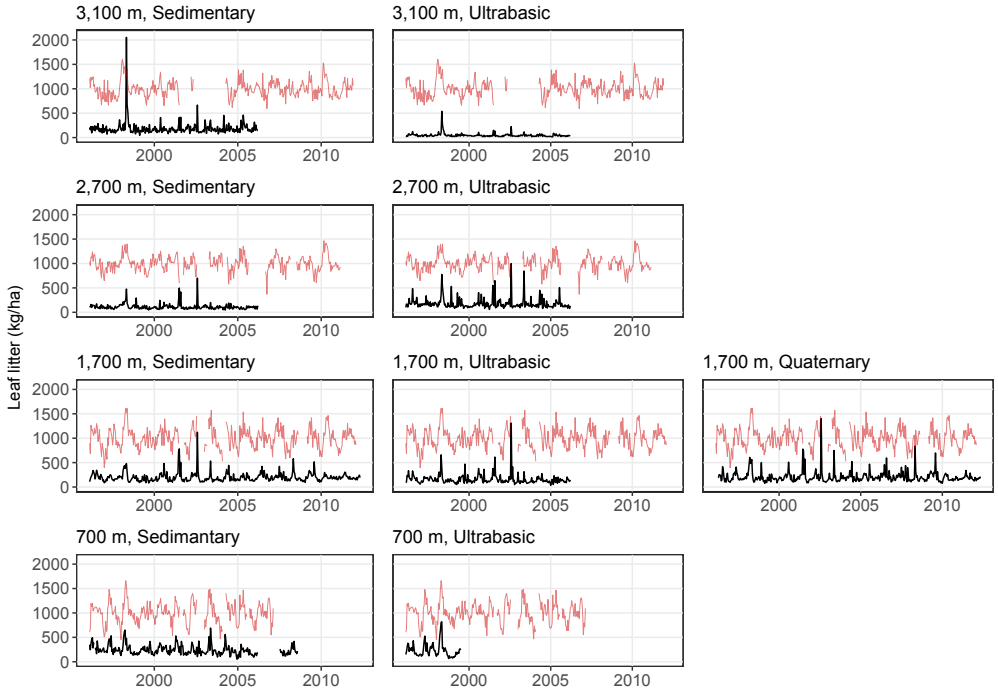

Figure 1: *Time series of leaf litter production in tropical rain forests on Mt. Kinabalu. Black lines indicate leaf litter production, and red lines indicate mean daily air temperature corrected by general additive model (only patterns are shown). The values on the y-axis is for leaf litter production.*

variables, a significant 12-mo periodicity was found for mean daily air temperature at 550, 1560, and 3270 m (Fig. 2e–h, Table S3), for mean daily relative humidity at all altitudes (550–3270 m), for daily potential evapotranspiration at 550 and 1560 m (Fig. 2g–h), and for photosynthetically active radiation (PAR) at 550 m only (Fig. 2h). Daily rainfall did not show a 12-mo periodicity at any altitude.

Although there is a distinct 1-year periodicity for leaf litterfall in most of our study sites, identifying the driver of the 1-year periodicity is not straightforward at all. This is because phase synchronization due to the shared periodicity easily generates clear correspondences between variables, which often leads to the misidentification of causality (e.g., Cobey et al. 2016). Recent accounts documenting long-term datasets of tropical phenology pointed out the need for novel analytical methods to identify a driver of the periodicity of flowering and fruiting (Morellato et al. 2018). Several methods have been proposed to overcome this limitation (Deyle et al. 2016, Ushio et al. 2018), but the issue is still unresolved. To overcome the limitation, we developed a novel analytical framework based on a previously developed causality test of empirical dynamic modeling (Sugihara et al. 2012). The idea is straightforward: if a variable is the driver of periodicity of another variable, then the fluctuation in the periodicity strength of the driver causes that of the effect variable. To implement the idea, we sequentially extract the strength of the 1-year periodicity using a moving window approach and Fourier analysis, and test whether variables cause the 1-year periodicity using a causality test of empirical dynamic modeling, convergent cross mapping (CCM) (Sugihara et al. 2012, Ye et al. 2015b) (see Methods and Fig. S5). Performance tests using simulation data showed that this method indeed distinguishes the true driver of seasonality from synchronized, non-driver variables (Figs. S5–S7). Because our approach tests the relationships among a spectrum of variables,

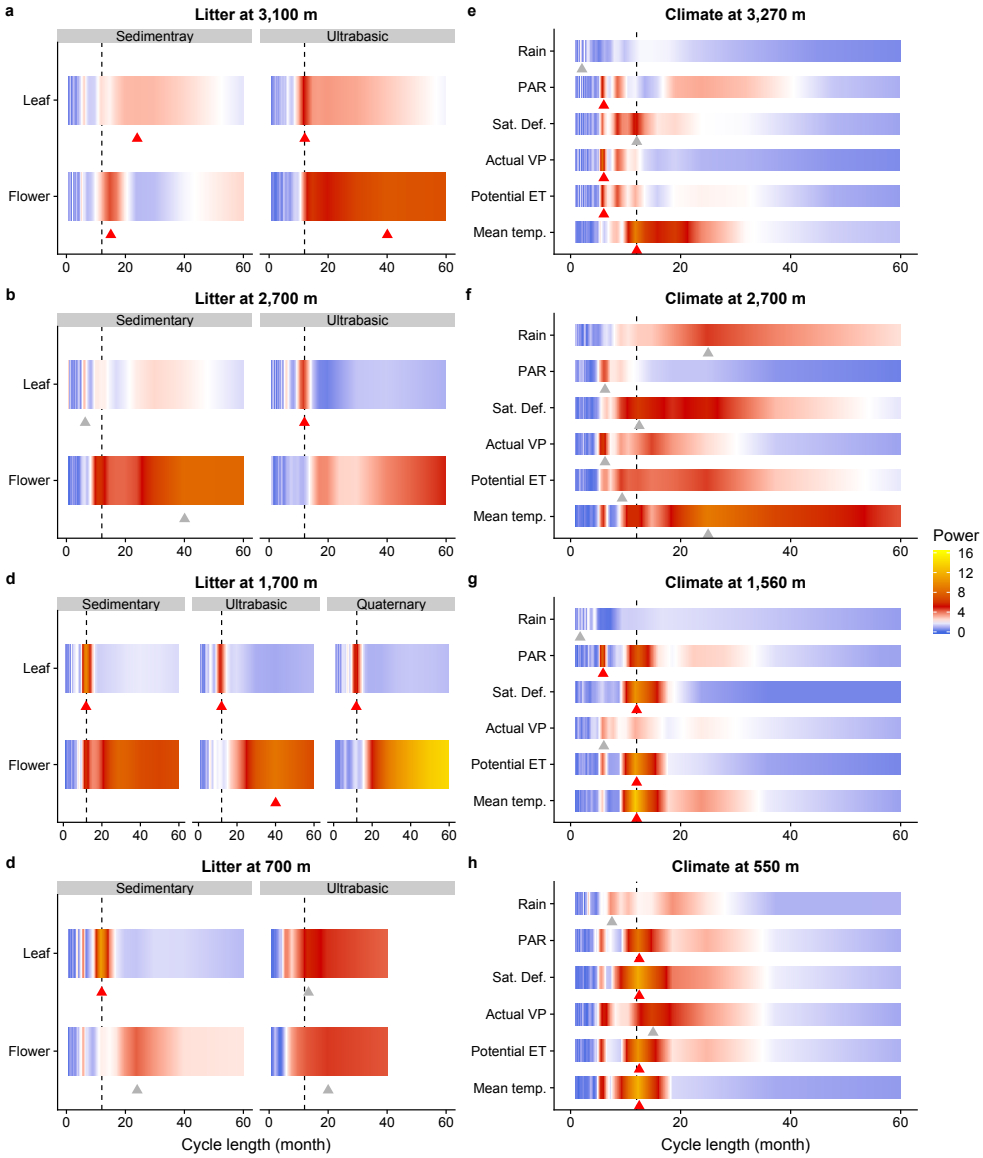

Figure 2: *Significance of the dominant cycle and spectrum of each time series. Spectrum of litter time series collected (**a**) at sedimentary/granite and ultrabasic sites at 3100 m, (**b**) at sedimentary and ultrabasic sites at 2700 m, (**c**) at sedimentary, ultrabasic and quaternary sites at 1700 m and (**d**) at sedimentary and ultrabasic sites at 700 m. Note that litter monitoring was abandoned at the ultrabasic site at 700 m after two years due to the site's extreme remoteness, and therefore the time series length is much shorter than those of the other sites. Spectrum of climate variables measured (**e**) at 3270 m, (**f**) 2700 m, (**g**) 1560 m, and (**h**) 550 m (corresponding to 3100 m, 2700 m, 1700 m and 700 m forest site, respectively). Mean temp., Potential ET, Actual VP, Sat. Def. and PAR indicate mean daily air temperature, potential evapotranspiration, actual vapor pressure, saturation deficit and photosynthetically active radiation, respectively. Dashed vertical line in each panel indicates the 1-year periodicity. Red and gray triangles indicate significant dominant periodicity and insignificant dominant periodicity at $P < 0.05$, respectively (see more details in Fig. S4). Dominant periodicity longer than 60 mo is not shown, but presented in Table S2 and S3. Gradient colours indicate the strength of the power.*

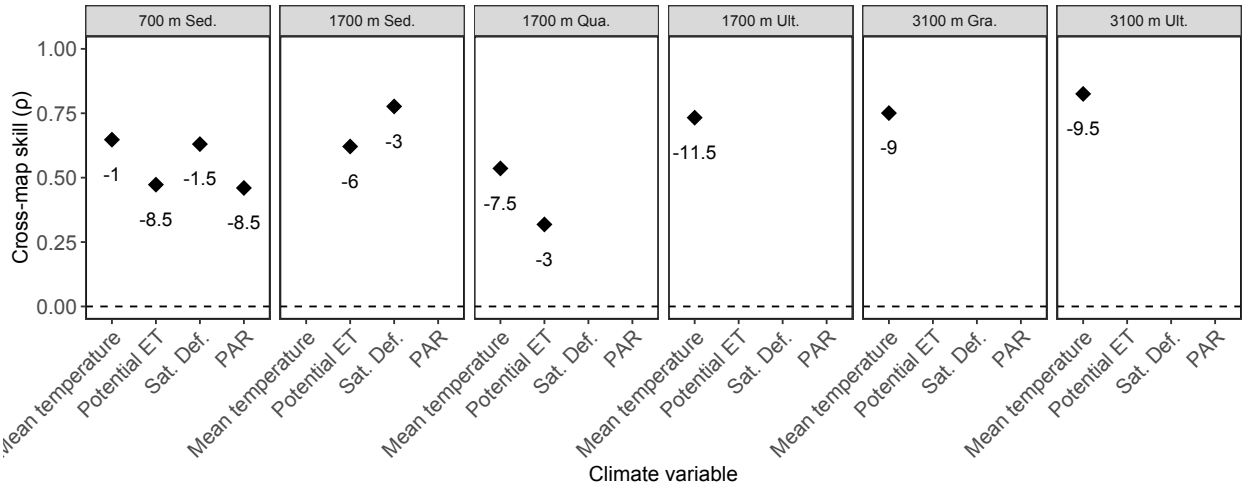

Figure 3: *Results of spectrum convergent cross mapping (spectrum CCM). Points indicate cross-map skills (ρ; correlation coefficient between observed values predicted by the cross-mapping). Only significant ($P < 0.05$) cross-map skills are shown. The number below each point indicates time-lag (months) of the significant cross-mapping. Labels on the x-axis indicate climate variables. The label on the top of each panel indicates the forest site.*

hereafter we name the approach "spectrum convergent cross mapping" (or "spectrum CCM").

The spectrum CCM analyses of the litterfall and meteorological datasets identify meteorological factors that cause the precise 1-year periodicity of leaf litterfall in the six forests. Mean daily air temperature is causally related to the annual periodicity of leaf litterfall across all forests except for the 1700-m sedimentary forest (Fig. 3). Time lags between responses (leaf litterfall dynamics) and signals (daily mean air temperature) range from -1 mo (leaf fall lags behind daily mean air temperature by 1 month) at 700 m to less than -7.5 mo (longer time lag than 7.5 months) at higher altitudes (Fig. 3). The 1-year periodicity of leaf litterfall in the 700-m sedimentary forest is causally related to potential evapotranspiration, saturation deficit and PAR in addition to mean daily air temperature. In addition, mean daily air temperature shows the highest cross-map skill (ρ) within each forest, suggesting that mean daily air temperature is a leading factor that drives the 1-year periodicity of leaf litterfall (Fig. 3).

The precise 1-year periodicity of mean daily air temperature is associated with the motion of the sun following the ecliptic. However, higher daily mean air temperatures occur in April–May in our sites (Fig. S3). This suggests that the yearly course of air temperature is most likely influenced by the movement of the intertropical convergence zone (ITCZ), which crosses the equator at equinoxes, causing more cloudy weather than usual, rather than by top-of-the-atmosphere radiation. The influence of ITCZ as a driver of the periodicity of flowering/fruiting has also been suggested in Panama (Wright and Calderón 2018). Another possible meteorological factor causing annual periodicity is the Asiatic monsoon. However, the monsoon changes year to year in magnitude and timing, and thus it is unlikely that the monsoon is a meteorological cue for the precise 1-year periodicity (Whitmore 1975). Mean daily air temperature as well as other meteorological variables including humidity and PAR show annual patterns in association with ITCZ, giving rise to precise 1-year periodicity of these meteorological variables. PAR, however, does not show annual periodicity at higher altitudes (above 1560 m, Fig. 2) and was not selected as a causative factor at higher

altitudes, suggesting that photoperiodicity is not a signal for leaf dynamics, unlike flowering elsewhere (Borchert et al. 2015). Photoperiodicity has been suggested to trigger synchronous flowering in the Amazon (Borchert et al. 2005). Tropical trees might have acquired adaptive responses of flowering to photoperiodicity, or to drought (Kobayashi et al. 2013), but not of vegetative growth, which is instead regulated by temperature. The detailed molecular mechanisms of the temperature control of the vegetative growth periodicity of equatorial tropical forests are still poorly understood. This is at least partly due to the much larger body size, much longer lifetime and higher diversity of tropical trees compared with those of temperate, herbaceous plants, including the model plant *Arabidopsis*, which consequently hinder the accumulation of genetic information. Although caution is needed because tropical trees may be different from *Arabidopsis*, molecular evidence from *Arabidopsis* systems may help to clarify mechanisms, and our findings are consistent with the hypothesis of decentralized circadian clocks in *Arabidopsis* (Shimizu et al. 2015), In *Arabidopsis*, circadian clocks function tissue-specifically with different meteorological signals. The circadian clock in vascular phloem companion cells is responsible for photoperiodic flowering, while that in leaf epidermis is responsible for temperature-dependent cell elongation (Shimizu et al. 2015). Leaf litterfall is closely linked to leaf extension in a canopy, because shoots (modules of leaves on a twig) are shed upon leaf extension. Thus, leaf litterfall is a proxy for leaf-cell elongation. Periodicity of leaf litterfall may be a result of the response of the circadian clock to temperature.

Although mean daily air temperature demonstrates sharp 12-mo periodicity, the mean annual amplitude of this periodicity is merely 2–3°C, with nearly 10°C daily oscillations. How plants respond to rather subtle annual temperature changes amid great daily oscillations is an intriguing question. In perennial *Arabidopsis halleri*, the expression of the flowering gene (a *FLOWRING LOCUS C* homolog) is significantly related to the accumulated temperature under a certain threshold temperature, indicating that phenological events are based on past temperature memory (Aikawa et al. 2010, Kudoh 2016). The altitude-dependent time lags between response (leaf fall) and signal (temperature) in Fig. 3 indicate the involvement of temperature memory based on accumulated temperature. Whether tropical trees respond to annual temperature changes by using past temperature memory needs to be answered by further ecological, genetic and statistical analyses.

Conclusions

Our results show that the periodicity of leaf literfall in equatorial tropical rain forests is determined by mean daily air temperature, which is celestially caused by the influence of the ITCZ. Because vegetative periodicity can be transmitted to the dynamics of higher trophic levels through a trophic cascade, interactions between vegetative periodicity and daily air temperature, not rainfall, would more strongly cause changes in the dynamics of forest ecosystems. Our results show that we need to redefine our concept of equatorial "aseasonal" tropical rain forests, and that daily air temperature is a more important factor than other climate variables in the climate-forest ecosystem interactions.

Methods

Study site

The study sites are located on Mount Kinabalu (summit height 4095 m; 6° 5′ N, 116 33′ E), Borneo, which is a non-volcanic mountain consisting of Tertiary sedimentary rocks of sandstone and/or mudstone below 3000 m and of granitic rock above 3000 m. Ultrabasic rocks also occur as mosaics below 3100 m. A pair of forests were selected on two contrasting geological substrates (one derived from sedimentary rock and the other derived from ultrabasic rock) each at 700, 1700, 2700 and 3100 m on the southern slope. The 3100-m "sedimentary" site is actually underlain by granitic rocks. These forests consist of a matrix of two soil types and four altitudes. In addition, we added a ninth forest at 1700 m on sedimentary substrate originated from Quaternary colluvium deposits. The structure and species composition of these forests were described in previous papers (Aiba and Kitayama 1999, Kitayama and Aiba 2002).

Litter and meteorological time-series data

Litterfall monitoring was performed from February 1996 until March 2006 or longer at all sites except for the 700-m ultrabasic site, where monitoring was abandoned after two years due to the site's extreme remoteness. Detailed descriptions of data collection are given in a previous paper (Kitayama and Aiba 2002). Briefly, a total of 20 litter traps at two lower altitudes, and a total of 10 traps at two higher altitudes were placed 1 m above the ground at 10 m intervals along 2 transects at each site. Traps were made of 1 mm mesh with an opening of 0.5 m^2 area, and were renewed annually. Field assistants collected trapped fine litter from each trap at two-week intervals without interruption from all sites. Collected litter was immediately oven-dried at 70°C for at least 3 days, sorted by trap into six fractions (leaves, reproductive organs including fruits and flowers, twigs $<$ 2 cm girth, epiphytes, palms and bamboos, and dust), and weighed to determine dry weight. We applied time-series analyses to each fraction in each forest.

Four automated meteorological stations were established at 550, 1560, 2700 and 3270 m on the south slope. Each station was located in an open place without obstacles within at least a 10 m radius. Each station consisted of climate sensors connected to a CR10x data logger (Campbell Scientific, Logan, Utah, USA); a Vaisala HMP35C probe for air temperature and relative humidity, a 107B probe for soil temperature (10 cm), a LI-COR 190SB quantum sensor for photosynthetically active radiation (PAR) (wavelength 400–700 nm), a TE525MM tipping bucket rain gauge for rainfall, and an RM Young 03001 Wind Sentry for wind speed/direction. Some of the sensors were renewed at regular intervals to prevent baseline drifts due to sensor deterioration; however, baseline drifts were still inevitable for PAR and humidity (see below concerning how drifts were removed). All readings were taken at 10-s intervals, and reduced to 30-min and 24-hour means and/or totals, and electronically stored in CR10x. Saturation deficits were calculated based on 30-min mean air temperature and instantaneous relative humidity values. Daily potential evapotranspiration was estimated following the Penman-Monteith equation (Allen et al. 1998).

Meteorological data correction

Daily mean saturation deficits and PAR still demonstrated baseline drifts due to sensor deterioration, which may influence the performance of time series analysis. The baseline drifts were, therefore,

corrected by constructing additive models using the "mgcv" package (Wood 2004) of R (R Core Team 2017). In the corrections, we assumed that the baseline drifts are long-term fluctuations in the climate variables, and that the additive models with the appropriate number of knots (k) can represent the long-term fluctuations. The additive models successfully represented the baseline drifts in the climate time series. Also, removing long-term trends made time series more stationary, which may allow better detection of dominant cycles and causality between time series. The residuals of the additive models do not include the long-term trends and were used as corrected climate time series for the subsequent time series analysis.

Fourier analysis

We performed a Fourier analysis to identify dominant cycles of meteorological and litter time series in the tropical forests (Bloomfield 2000). Fourier analysis is a spectral analysis used to decompose a time series into sine waves of different frequencies. Because Fourier analysis requires consecutive time series (i.e., missing values are not allowed), we selected a longest consecutive time series (Table S1). As meteorological time series sometimes contain missing values, a maximum of six consecutive missing values were interpolated by using simple linear interpolation. For litter time series, there were no missing values. Bush et al. (2017) proposed a practical procedure to detect a dominant cycle from a given time series, and we generally followed that method. First, the raw spectral estimates were smoothed using the modified Daniell kernel. We adjusted the width of the Daniell kernel so that a bandwidth become approximately 0.1, which was found to give sufficient resolution to identify a dominant peak (Bush et al. 2017). The significance of the dominant peak was tested by calculating 95% confidence intervals, assuming that spectral estimates approximate a chi-square distribution (Bloomfield 2000). We rely on the null continuum of the spectrum (i.e., the null spectrum) as a null hypothesis rather than the average spectrum (i.e., white noise spectrum) because the null spectrum showed fewer false positive results (Bush et al. 2017). See Tables S2 and S3 for the summary of Fourier analysis.

Time series of seasonality and the framework of spectrum convergent cross mapping (spectrum CCM)

As presented in the main text, our analysis showed that the dominant cycles of meteorological and litter (especially, leaf litter) time series were 12 months (i.e., annual cycle) at many sites. Synchronized seasonality often makes detection of causality extremely difficult. Indeed, previous studies showed that synchronization driven by seasonality can lead to misidentification of causality (i.e., false-positive detection of causality) (e.g., Cobey et al. 2016, Supporting Information in Ushio et al. 2018). More importantly, even if a causal variable is identified, the variable may not necessarily be a driver of "seasonality". For example, if a causal variable influences only during a certain period of the year, then the variable only slightly contributes to the whole seasonality of an effect variable. Such variable is a causal factor, but not a driver of seasonality of a response variable.

To overcome this problem, here we introduce spectrum convergent cross mapping (spectrum CCM) as a general approach to detect a driver of seasonality among highly synchronized time series. The idea is straightforward: if a time series is a driver of seasonality of another time series, then the seasonality of the causal time series drives the seasonality of the effect time series. Strength of seasonality, which can be quantified as the power of an annual cycle (i.e., the amplitude of seasonality), can also be a time series if we sequentially calculate using a moving window method,

and thus CCM, a causality test of empirical dynamic modeling (EDM) (Sugihara et al. 2012), allows to detect causality among the powers of seasonality (for the algorithm of CCM, see the section below).

Time series of seasonality were generated as follows (Fig. S5): (1) A 3-year window was set in an original time series, (2) Fourier analysis was performed for the 3-year time series, (3) the power of annual cycle (i.e., seasonality) was extracted, (4) steps 1–3 were sequentially performed for the whole time series, and (5) the obtained time series were then first-differentiated to make the time series stationary. Briefly, when the total length (time point) of time series X with time interval at 2-weeks is N, the ith 3-year window is described as follows,

$$X = [X(1), X(2), ..., X(i+71)]$$

$$X_i = [X(i), X(i+1), \ldots, X(i+71)]$$

where $X(i)$ indicates the ith element of the time series and X_i should contain $24 \times 3 = 72$ elements corresponding to the 3-year term (Fig. S5a). In total, we obtain $N - 71$ of X_i and Fourier analysis is applied to each X_i, resulting in $N - 71$ powers of the 1-year periodicity (Fig. S5b). Let the power of the 1-year periodicity of X_i be $S(i)$ and time series of $S(i)$ be S, and then the first-differentiated S is described as follows (Fig. S5c,d),

$$S = [S(1), S(2), \ldots, S(N-71)]$$

$$S_{diff} = [S(2) - S(1), S(3) - S(2), \ldots, S(N-70) - S(N-71)]$$

S_{diff} is normalized to zero mean and unit variance and then used as an input for CCM explained in the next subsection.

Convergent cross mapping (CCM)

Causalities among the first-differentiated time series of seasonality were tested with convergent cross mapping (CCM) (Sugihara et al. 2012). CCM is based on Takens' theorem for nonlinear dynamical systems (Takens 1981). Consider a multi-variable dynamical system, in which only some of variables are observable. Takens' theorem (Takens 1981), with several extensions (Deyle and Sugihara 2011, and references therein), proved that it is possible to represent the system dynamics in a state space by substituting time lags of the observable variables for the unknown variables. The information in the unobservable variables is encoded in the observed time series, and so a single time series can be used to reconstruct the original state space. This gives a time-delayed coordinate representation (or embedding) of the system trajectories, and this operation is referred to as state space reconstruction (SSR). For example, consider a multi-variable system including a variable X. Even if other variables involved in the system are unobserved, the time-delayed embedding of X, $[X(t), X(t-1), X(t-2), \ldots, X(t-(E-1))]$ where E is the embedding dimension, represent the whole dynamics of the multi-variable system. EDM (and thus CCM) is based on SSR, and recent studies demonstrated that EDM is a useful tool to analyze nonlinear dynamics in natural ecosystems (Ye et al. 2015a, 2015b, Deyle et al. 2016, Chang et al. 2017, Ushio et al. 2018).

An important consequence of the SSR theorems is that if two variables are part of the same dynamical system, then the reconstructed state spaces of the two variables will represent topologically the same attractor (with a one-to-one mapping between reconstructed attractors). Therefore, it is possible to predict the current state of a variable using time lags of another variable. We can look for the

signature of a causal variable in the time series of an effect variable by testing whether there is a correspondence between their reconstructed state spaces (i.e., cross mapping). Cross-map skill is evaluated by a correlation coefficient (ρ) between observed and predicted values by cross mapping. In addition, the cross-map skill will increase as the library length (i.e., the number of points in the reconstructed state space of an effect variable) increases if two variables are causally related (i.e., convergence). In this study, cross mapping from one variable to another was performed using simplex projection. How many time lags are taken in SSR (i.e, embedding dimension) is determined by simplex projection using mean absolute error as an index of forecasting skill. More detailed algorithms about simplex projection and cross mapping can be found in previous studies (Sugihara et al. 2012, Ye et al. 2015a, 2015b, Deyle et al. 2016, Ushio et al. 2018).

In this study, the significance of CCM is judged by comparing cross-map skill and convergence of Fourier surrogates and original time series. More specifically, first, 1000 surrogate time series for one original time series are generated. Second, cross-map skill (ρ) and convergence (i.e., the difference between cross-map skills (ρ) at the minimum and maximum library lengths) are calculated for 1000 surrogate time series and the original time series. If the number of surrogates that shows a higher ρ as well as a higher convergence is less than 50 (i.e., 5% of the surrogates), the cross mapping is judged as significant. Hereafter, the number of surrogates that shows a higher ρ as well as a higher convergence is referred to as "joint P-value".

Performance test of spectrum CCM

To evaluate the performance of the newly developed spectrum CCM, we performed a simulation test. In the simulation, we prepare four time series, including one response time series and three explaining time series with shared seasonality: 1) one time series continuously influences the response time series (time series A), 2) one time series influences the response time series during only a certain period of the year (time series B), and 3) one time series does not influence the response time series (time series C) (Fig. S5e, f). Time series A, B, and C are generated by adding a sine curve to the exponential of random values taken from a normal distribution. The amplitude of the sine curve added is defined as the strength of seasonality.

In a mathematical expression, model time series A is generated as follows:

$$R_{A,0} \sim N(0,1)$$

$$R_A = e^{R_{A,0}}$$

where $R_{A,0}$ is random values that follow the normal distribution, and R_A is the exponential of $R_{A,0}$. Seasonality is then added to make time series with shared seasonality.

$$T_A = \beta_{1,A} \times R_A + \beta_{2,A} \times Seasonality ...(1)$$

where T_A is a generated model time series A, $\beta_{1,A}$ and $\beta_{2,A}$ define the relative strength of random values and seasonality, respectively, and Seasonality is defined by a sine curve ($\beta_{1,A} = 1$ in the simulation). Importantly, we add a small fluctuation in $\beta_{2,A}$ (i.e., coefficient of variation of $\beta_{2,A}$ is 20%) depending on time because the strength of seasonality can change in nature (this is also evident in our results). Model time series B and C are generated in the same way.

The response time series, T_R, is generated by combining a logistic map and influences from time series A (T_A) and B (T_B).

$$T_{R,0}(t+1) = T_{R,0}(t) \times (3.8 - 3.8 \times T_{R,0}(t))$$

$$T_R(t+1) = a \times T_{R,0}(t+1) + b \times (T_A(t) - \Theta(t) \times T_B(t)) \ldots (2)$$

where $T_{R,0}$ is the internal dynamics that is not influenced by external factors, and T_R is observed values that include influences from external factors (e.g., climate factors). As shown in Eqn. (2), T_A and T_B have causal influences on T_R. As a is always one in the simulation, the relative influences of T_A and T_B are determined by b ($b = 2$ in the simulation). The period when T_B has influence on T_R is determined by $\Theta(t)$, where $\Theta(t)$ denotes the Heaviside function ($\Theta(t)$ is 0 when t is the first three-fourths of a year, and is 1 during the last one-fourth of a year). Therefore, T_B has causal influences on T_R only during the last one fourth of a year (i.e., periodic influence). On the other hand, T_A always has causal influences on T_R and thus is regarded as a major driver of the seasonality of T_R. T_C has no influence on T_R, but unlike spectrum CCM, T_C with strong (shared) seasonality is sometimes incorrectly identified as a causal factor when using normal CCM (Figs. S6, S7).

For the performance test, we generated model time series with different seasonality strengths (i.e., $\beta_{2,i}$, where i is either of A, B, or C; a relative amplitude of sine curve compared with non-seasonal variation) and different observation errors. We applied 11 seasonality strengths (i.e., $\beta_{2,i}$ is changed from 0 [no seasonality] to 2 [strong seasonality]; in R script, seq(0, 2.0, by=0.2); see Fig. S5 for example time series) and 11 observation errors (i.e., from 0% to 50% of standard deviation of the time series; in R script, seq(0, 0.5, by=0.05)) and the number of the four time series sets is 100 for each test. The interval of time series is two weeks, and the length of the time series is 12 years (288 time points).

For the model time series (i.e., the response time series and three explaining time series), we performed two tests. First, spectrum CCM was applied to the set of the four time series, and we examined the joint P-value (mean joint P-value of 100 replicates) and detection probability (the proportion of time series that identified the driver of seasonality of the response time series). Second, normal CCM was applied to the set of the four time series as a comparison (i.e., raw time series were used in CCM). Time-lag paramter of CCM is preliminary determined and one-step time-lag (i.e., tp = -1 in rEDM functions in R script) is used throughout the simulation (i.e, lagged CCM, Ye et al. 2015b). In total, we performed 12 100 000 CCMs for spectrum CCM and normal CCM, respectively (100 replicates of model time series $\times$ 11 seasonality strengths $\times$ 11 observation errors $\times$ 1000 surrogates for significance test = 12 100 000).To evaluate the performance, mean joint P-value of 100 replicates and detection probability (= the number of replicates of which joint P-value < 0.05 / 100 replicates) were calculated.

Spectrum CCM correctly identified the true seasonality driver at most 20-30% of observation errors when the time series showed relatively weak to strong seasonality (Fig. S6). Also, spectrum CCM does not detect time series B and C (i.e., periodic influencer and non-driver) as the driver of seasonality (a low possibility of the false-positive detection; Fig. S6). Normal CCM always detects time series A as a significant driver of seasonality (Fig. S7). However, normal CCM often detects time series B (a periodic influencer) as the driver of seasonality, especially when the strength of seasonality is weak (i.e., a high possibility of false-positive detection; Fig. S7). Also, the test showed that, even time series C (a non-causal, random value time series) may be detected as the driver of seasonality when they are synchronized (Fig. S7).Overall, spectrum CCM is a much more conservative method for detecting the driver of seasonality when time series are synchronized due

to shared seasonality. The strength of seasonality of our time series data that showed significant 1-yaer periodicity is approximately in a range of relatively weak to modest seasonality (Figs. 1, S5e), and thus the application of spectrum CCM to our data enables robust detection of a driver of seasonality.

Computation

CCM was performed using the "rEDM" package (version 0.6.9) (Ye et al. 2015a), and all statistical analyses were performed in the free statistical environment R v3.4.3 (R Core Team 2017).

Code and data availability

Time-series of leaf and flower litter of the nine forests on Mount Kinabalu will be available after the formal acceptance of this manuscript at https://github.com/ong8181. The scripts used for the main analyses will be available at https://github.com/ong8181.

Supplementary information

Supplementary information is available for this paper.

Author contributions

K.K. and S.A. designed the litter monitoring and collected data; K.K. and M.U. conceived the hypothesis; M.U. invented the spectrum CCM; M.U analysed data with contribution from K.K.; K.K. and M.U. wrote the first draft; all authors were involved in interpretation, discussion and final writing.

Acknowledgements

We thank Dr. Jamili Nais and Puan Rimi Repin of Sabah Parks, who have been encouraging the litter monitoring, and all other field assistants who assisted with monitoring and sample collection. This study was supported by the Global Environment Research Funds B-52 and B-11 of the Ministry of the Environment to K.K.

References

Adamescu, G. S., A. J. Plumptre, K. A. Abernethy, L. Polansky, E. R. Bush, C. A. Chapman, L. P. Shoo, A. Fayolle, K. R. L. Janmaat, M. M. Robbins, H. J. Ndangalasi, N. J. Cordeiro, I. C. Gilby, R. M. Wittig, T. Breuer, M. B.-N. Hockemba, C. M. Sanz, D. B. Morgan, A. E. Pusey, B. Mugerwa, B. Gilagiza, C. Tutin, C. E. N. Ewango, D. Sheil, E. Dimoto, F. Baya, F. Bujo, F. Ssali, J.-T. Dikangadissi, K. Jeffery, K. Valenta, L. White, M. Masozera, M. L. Wilson, R. Bitariho, S. T. Ndolo Ebika, S. Gourlet-Fleury, F. Mulindahabi, and C. M. Beale. 2018. Annual cycles are the most common reproductive strategy in African tropical tree communities. Biotropica 50:418–430.

Aiba, S., and K. Kitayama. 1999. Structure, composition and species diversity in an altitude-substrate matrix of rain forest tree communities on Mount Kinabalu, Borneo. Plant Ecology 140:139–157.

Aikawa, S., M. J. Kobayashi, A. Satake, K. K. Shimizu, and H. Kudoh. 2010. Robust control of the seasonal expression of the Arabidopsis FLC gene in a fluctuating environment. Proceedings of the National Academy of Sciences of the United States of America 107:11632–11637.

Allen, R., L. Pereira, D. Raes, and M. Smith. 1998. Crop evapotranspiration —guidelines for computing crop water requirements. FAO - Food; Agriculture Organization of the United Nations Rome.

Bloomfield, P. 2000. Fourier Analyis of Tiime Series: An Introduction. 2nd editions. John Wiley & Sons, New York, USA.

Borchert, R., Z. Calle, A. H. Strahler, A. Baertschi, R. E. Magill, J. S. Broadhead, J. Kamau, J. Njoroge, and C. Muthuri. 2015, January. Insolation and photoperiodic control of tree development near the equator.

Borchert, R., S. S. Renner, Z. Calle, D. Navarrete, A. Tye, L. Gautier, R. Spichiger, and P. von Hildebrand. 2005. Photoperiodic induction of synchronous flowering near the Equator. Nature 433:627–629.

Bush, E. R., K. A. Abernethy, K. Jeffery, C. Tutin, L. White, E. Dimoto, J.-T. Dikangadissi, A. S. Jump, and N. Bunnefeld. 2017. Fourier analysis to detect phenological cycles using long-term tropical field data and simulations. Methods in Ecology and Evolution 8:530–538.

Chang, C.-W., M. Ushio, and C.-h. Hsieh. 2017. Empirical dynamic modeling for beginners. Ecological Research 32:785–796.

Cobey, S., E. B. Baskerville, H. Abarbanel, T. Carroll, C. hao Hsieh, and L. Richards. 2016. Limits to Causal Inference with State-Space Reconstruction for Infectious Disease. PLOS ONE 11:e0169050.

Deyle, E. R., M. C. Maher, R. D. Hernandez, S. Basu, and G. Sugihara. 2016. Global environmental drivers of influenza. Proceedings of the National Academy of Sciences of the United States of America 113:13081–13086.

Deyle, E. R., and G. Sugihara. 2011. Generalized theorems for nonlinear state space reconstruction. PLOS ONE 6:e18295.

Kitayama, K., and S. Aiba. 2002. Ecosystem structure and productivity of tropical rain forests along altitudinal gradients with contrasting soil phosphorus pools on Mount Kinabalu, Borneo. Journal of Ecology 90:37–51.

Kobayashi, M. J., Y. Takeuchi, T. Kenta, T. Kume, B. Diway, and K. K. Shimizu. 2013. Mass flowering of the tropical tree Shorea beccariana was preceded by expression changes in flowering and drought-responsive genes. Molecular ecology 22:4767–4782.

Kudoh, H. 2016. Molecular phenology in plants: in natura systems biology for the comprehensive understanding of seasonal responses under natural environments. The New phytologist 210:399–412.

Lodge, D. J., W. H. McDowell, and C. P. McSwiney. 1994. The importance of nutrient pulses in tropical forests. Trends in Ecology & Evolution 9:384–387.

Morellato, L. P. C., K. Abernethy, and I. Mendoza. 2018. Rethinking tropical phenology: insights from long-term monitoring and novel analytical methods. Biotropica 50:371–373.

R Core Team. 2017. R: A Language and Environment for Statistical Computing. R Foundation for Statistical Computing, Vienna, Austria.

Reich, P. B., C. Uhl, M. B. Walters, L. Prugh, and D. S. Ellsworth. 2004. Leaf demography and phenology in Amazonian rain forest: A census of 40000 leaves of 23 tree species. Ecological Monographs 74:3–23.

Rivera, G., S. Elliott, S. L. Caldas, G. Nicolossi, T. V. Coradin, and R. Borchert. 2002. Increasing day-length induces spring flushing of tropical dry forest trees in the absence of rain. Trees 16:445–456.

Sakai, S. 2002. General flowering in lowland mixed dipterocarp forests of South-east Asia. Biological Journal of the Linnean Society 75:233–247.

Sakai, S., R. D. Harrison, K. Momose, K. Kuraji, H. Nagamasu, T. Yasunari, L. Chong, and T. Nakashizuka. 2006. Irregular droughts trigger mass flowering in aseasonal tropical forests in asia. American journal of botany 93:1134–1139.

Sakai, S., K. Momose, T. Yumoto, T. Nagamitsu, H. Nagamasu, A. A. Hamid, and T. Nakashizuka. 1999. Plant reproductive phenology over four years including an episode of general flowering in a lowland dipterocarp forest, Sarawak, Malaysia. American journal of botany 86:1414–1436.

Shimizu, H., K. Katayama, T. Koto, K. Torii, T. Araki, and M. Endo. 2015. Decentralized circadian clocks process thermal and photoperiodic cues in specific tissues. Nature Plants 1:15163.

Sugihara, G., R. May, H. Ye, C.-h. Hsieh, E. Deyle, M. Fogarty, and S. Munch. 2012. Detecting causality in complex ecosystems. Science 338:496–500.

Takens, F. 1981. Detecting strange attractors in turbulence. Pages 366–381 *in* D. Rand and L.-S. Young, editors. Dynamical systems and turbulence.

Ushio, M., C.-h. Hsieh, R. Masuda, E. R. Deyle, H. Ye, C.-W. Chang, G. Sugihara, and M. Kondoh. 2018. Fluctuating interaction network and time-varying stability of a natural fish community. Nature 554:360–363.

Whitmore, T. C. 1975. Tropical Rain Forests of the Far East. Page 282. Oxford University Press.

Wood, S. N. 2004. Stable and efficient multiple smoothing parameter estimation for generalized additive models. Journal of the American Statistical Association 99:673–686.

Wright, S. J., and O. Calderón. 2018. Solar irradiance as the proximate cue for flowering in a tropical moist forest. Biotropica 50:374–383.

Ye, H., R. J. Beamish, S. M. Glaser, S. C. H. Grant, C.-H. Hsieh, L. J. Richards, J. T. Schnute, and G. Sugihara. 2015a. Equation-free mechanistic ecosystem forecasting using empirical dynamic modeling. Proceedings of the National Academy of Sciences of the United States of America 112:E1569–E1576.

Ye, H., E. R. Deyle, L. J. Gilarranz, and G. Sugihara. 2015b. Distinguishing time-delayed causal interactions using convergent cross mapping. Scientific Reports 5:14750.